Dissecting motility signaling through activation of specific Src-effector complexes

Andrei V Karginov[1,4], Denis Tsygankov[1], Matthew Berginski[2], Pei-Hsuan Chu[1], Evan D Trudeau[1], Jason J Yi[1], Shawn Gomez[3], Timothy C Elston[1] & Klaus M Hahn[1,3]*

We describe an approach to selectively activate a kinase in a specific protein complex or at a specific subcellular location within living cells and within minutes. This reveals the effects of specific kinase pathways without time for genetic compensation. The new technique, dubbed rapamycin-regulated targeted activation of pathways (RapRTAP), was used to dissect the role of Src kinase interactions with FAK and p130Cas in cell motility and morphodynamics. The overall effects of Src activation on cell morphology and adhesion dynamics were first quantified, without restricting effector access. Subsets of Src-induced behaviors were then attributed to specific interactions between Src and the two downstream proteins. Activation of Src in the cytoplasm versus at the cell membrane also produced distinct phenotypes. The conserved nature of the kinase site modified for RapRTAP indicates that the technique can be applied to many kinases.

Protein kinases regulate cell behaviors by activating multiple downstream pathways in parallel. Downstream players act synergistically, controlling different aspects of the cellular machinery, so the role of specific kinase interactions is difficult to decipher. Small-molecule kinase inhibitors affect all of the pathways downstream of the kinase and often cannot target one kinase among similar isoforms. Genetic manipulations are prone to cell compensation and provide only poor temporal resolution. None of these methods couple the ability to activate a specific kinase with the ability to restrict kinase interaction to one downstream target.

Src is a ubiquitous protein important in a wide array of cell behaviors[1], including normal motility and metastasis[1–3], but little is known about the immediate effects of Src activation or which downstream molecules mediate which Src effects. Src regulates multiple cellular processes by signaling in different protein complexes and at different subcellular locations. Membrane targeting via N-terminal myristoylation of Src is required for Src-mediated oncogenic transformation and normal motility, but there is a substantial pool of Src in the cytoplasm, whose role remains unknown[4–9]. This cytosolic Src can potentially interact with proteins important for morphodynamics at focal adhesions or the cytoskeleton[10]. In this study, we examine specific effects of Src signaling through focal adhesion kinase (FAK) and p130Cas to control cell morphology and migration[3,11,12]. Both interactions are known to have a role in motility, but the specific events triggered by each remained obscure.

To rapidly activate a kinase in complex with a single specific target, we built upon our previously described RapR approach for kinase activation[13,14]. RapR kinases are made by inserting a modified FK506-binding protein (iFKBP) into a highly conserved portion of the kinase catalytic domain, inactivating the kinase. Addition of rapamycin leads to heterodimerization of the inserted iFKBP with a coexpressed FKBP12-rapamycin–binding domain (FRB), causing kinase reactivation. Though valuable, this approach leads to interaction of the kinase with all downstream targets indiscriminately.

Here, by fusing a modified FRB to a specific kinase target, activation was restricted to that kinase-target interaction alone (**Fig. 1a**). The new technique, dubbed RapR-TAP, enabled us to dissect the role of Src interactions with specific downstream effectors or, by localizing the FRB, compare effects of Src activation at different subcellular locations.

RESULTS

Morphological changes stimulated by the activation of Src

Using a rapamycin-inducible Src (RapR-Src)[13], we first characterized the cell activities produced simply by Src activation without directing Src to specific targets. These behaviors could later be compared with those produced when RapRTAP was used to restrict Src activation to specific protein complexes or subcellular locations. To ensure that Src was activated only by rapamycin and was not subject to upstream regulation, we used the Y529F mutant[15] of the RapR-Src construct. Activation of RapR-Src in HeLa cells led to cell spreading, an increase in the number and length of filopodia and an increase in the number of adhesions accompanied by adhesion elongation (**Fig. 1b–d** and **Supplementary Results**, **Supplementary Videos 1–4**). Spreading was quantified as the total change in cell area, and protrusive activity was measured as the sum of the areas associated with regions of the cell that undergo local extensions between subsequent movie frames (**Supplementary Fig. 1**). Adhesion number and shape were assessed using a previously published method[16]. To quantify filopodia dynamics, we applied a computational method that allows accurate identification and tracking of all cellular protrusions of arbitrarily complex shape (**Supplementary Fig. 2**). The method, which represents the cell boundary as a tree graph, allows unambiguous specification of filopodia and, notably, works for cells and protrusions of any scale and geometry in an unbiased automated manner (Online Methods).

All of the quantified changes began within 2–4 min of Src activation (**Supplementary Figs. 3–5**). The area of the HeLa cells increased 25–30% (**Supplementary Fig. 3a**). The increase in

[1]Department of Pharmacology, University of North Carolina at Chapel Hill, Chapel Hill, North Carolina, USA. [2]Department of Biomedical Engineering, University of North Carolina at Chapel Hill, Chapel Hill, North Carolina, USA. [3]Lineberger Cancer Center, University of North Carolina at Chapel Hill, Chapel Hill, North Carolina, USA. [4]Present address: Department of Pharmacology, University of Illinois at Chicago, Chicago, Illinois, USA. *e-mail: khahn@med.unc.edu
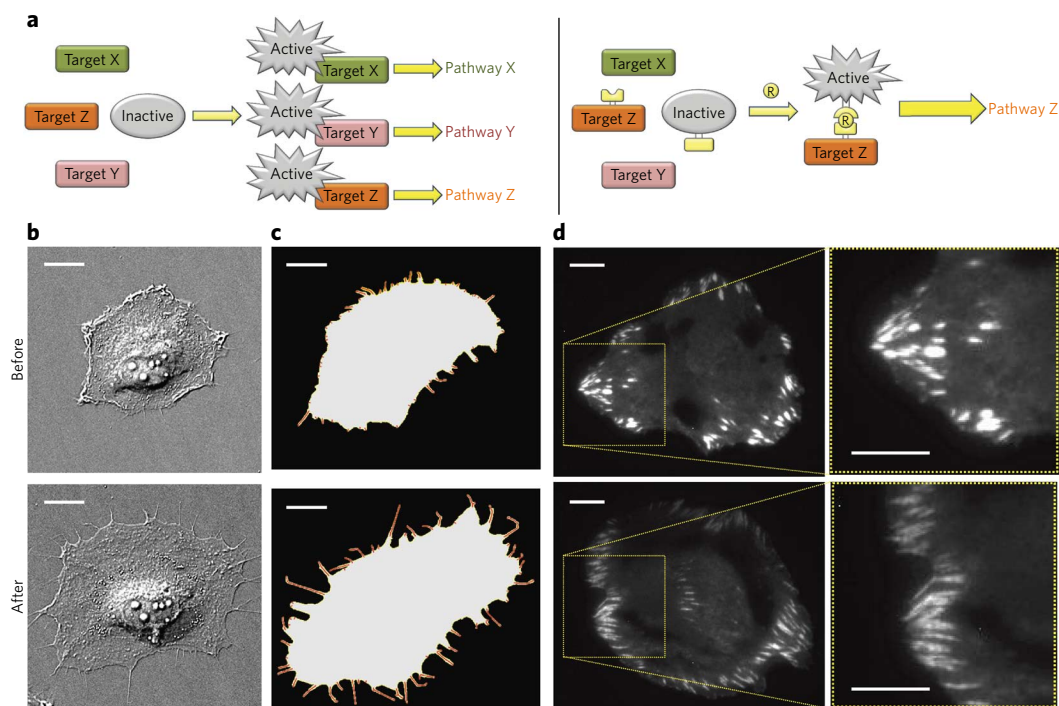
Figure 1 | RapRTAP design and Src-induced morphological changes. (**a**) Unlike wild-type kinases that are subject to complex upstream regulation and interact with multiple downstream targets (left), with RapR-TAP, a specific kinase is activated to interact with only one specific target (right). Activation occurs when addition of rapamycin leads to interaction of two engineered domains (yellow), one on the kinase and the other on the target. (**b**–**d**) Before using RapRTAP to attribute specific roles to different Src interactions, the overall effects of Src were characterized by activating Src without targeting a specific effector protein. This produced spreading (**b**), filopodia formation and lengthening (**c**) and rearrangement of focal adhesions (**d**). Kinetics and quantification of these phenotypes are shown in **Supplementary Figures 3–5**. HeLa cells transiently coexpressing RapR-Src and FRB were imaged before and after addition of rapamycin. Cells were transiently transfected together with mCherry-stargazin to visualize the cell membrane in **c** and with mCherry-paxillin to detect focal adhesions using TIRF microscopy in **d**. Scale bars for **b** and **c** correspond to 20 µm. Scale bars for **d** correspond to 10 µm.

area was produced by a transient burst of protrusive activity that subsided after roughly 40 min (**Supplementary Fig. 3b**). Filopodia increased two- to threefold in density along the cell edge and grew roughly 50% longer. These changes plateaued after roughly 20 min (**Supplementary Fig. 4**). Adhesions increased in number by 80% and became more filamentous and elongated (**Supplementary Fig. 5**). The change in adhesion number coincided with the period of rapid cell spreading. Control studies showed that these changes were specifically due to Src activity. The kinase-inactive mutant of RapR-Src (D388R) did not produce any discernible change in cell area, protrusive activity or filopodia (**Supplementary Figs. 3–5**). Similarly, no effects were observed in cells that were not transfected with any Src constructs (**Supplementary Figs. 3–5**).

A series of controls ensured that the effects we observed were solely due to RapR-Src: Activation of RapR-Src with rapamycin increased the phosphorylation of the Src substrates paxillin, p130Cas and FAK and led to robust autophosphorylation of RapR-Src on Tyr418, a known indicator of Src activation[1,15] (**Supplementary Figs. 6** and **7**). Rapamycin produced little or no Tyr418 phosphorylation of endogenous Src (**Supplementary Fig. 6**). Cells not expressing RapR-Src or expressing kinase-inactive RapR-Src showed no discernible change in phosphorylation of paxillin, p130Cas, FAK or endogenous Src Tyr418 upon rapamycin treatment. Expression of kinase-inactive RapR-Src did not discernibly affect the expression level or Tyr418 phosphorylation of endogenous Src. (**Supplementary Fig. 6**). Localizations of active and inactive RapR-Src were like those previously described for wild-type Src[10,17,18] (**Supplementary Fig. 8**). Rapamycin was not added until the cells had already reached their maximum

area during normal plating, indicating that Src activity alone was sufficient to promote additional spreading.

Membrane versus cytoplasmic Src activation

To parse out the roles of Src that require membrane translocation, we mutated RapR Src to eliminate the myristoylation required for membrane binding (G2A mutant)[19] and then compared activation using either soluble cytosolic FRB or FRB anchored to the membrane by the Src N-terminal myristoylation domain (N-terminal 11 amino acids[20]; **Fig. 2a**). The G2A mutation of RapR-Src did not affect its catalytic activity (**Supplementary Fig. 9**).

Activation of Src targeted to the plasma membrane led to robust spreading, as shown by a burst of protrusive activity and corresponding increase in cell area even greater than that seen upon activation of Src alone (**Fig. 2b**–**d** and **Supplementary Video 5** and **Supplementary Figs. 10** and **11**). To our surprise, Src activated without membrane anchoring was also able to induce protrusive activity, but, in contrast to membrane-anchored Src, protrusive activity never ceased, and activation did not lead to an increase in cell area (**Fig. 2b**–**d** and **Supplementary Video 6** and **Supplementary Figs. 10** and **11**). Only the membrane-anchored Src was able to produce a substantial increase in adhesion number (**Fig. 2e** and **Supplementary Fig. 12**), suggesting feedback in which protrusive activity is halted when adhesion formation leads to stable protrusions. Filopodia production required Src membrane localization, suggesting different pathways for lammelipodial versus filopodial protrusion (**Fig. 2f,g** and **Supplementary Figs. 13** and **14**). Focal adhesion shape changes were produced only by activation of non-myristoylated Src (**Fig. 2h** and **Supplementary Fig. 15**).
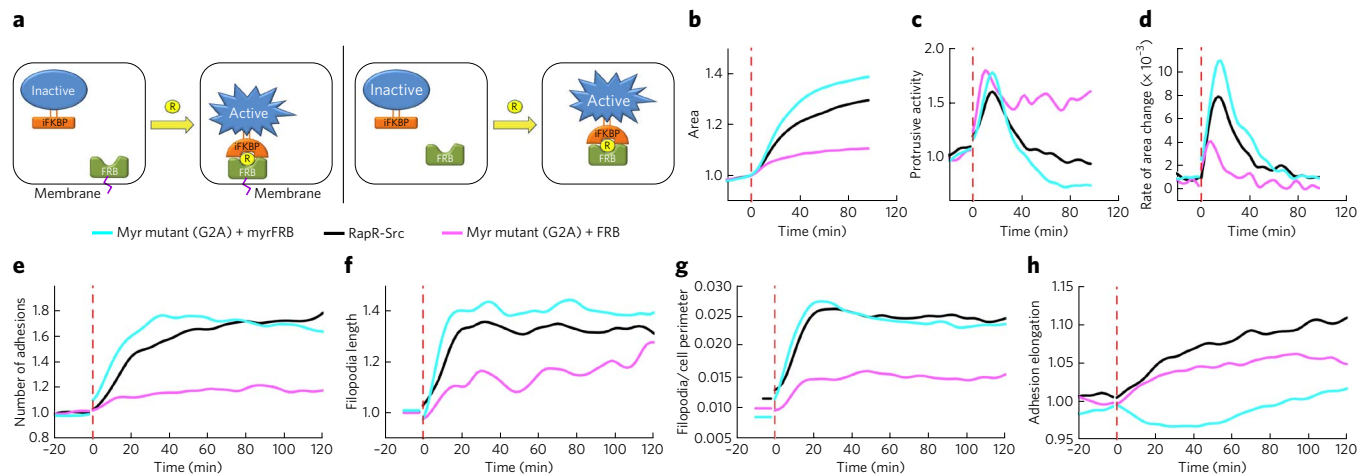
Figure 2 | Restricting the activation of Src to specific subcellular locations. (**a**) The nonmyristoylated, cytoplasmic mutant of RapR-Src (G2A) was activated only when complexed with FRB. Membrane-anchored FRB (left) versus free FRB in cytoplasm (right) produced different Src-induced phenotypes. (**b–h**) Quantitative assays of phenotypes induced by Src activation (Online Methods and **Supplementary Figs. 1** and **2**): cell spreading (**b**), protrusive activity (**c**), rate of area change (**d**), number of focal adhesions (**e**), filopodia length (**f**), filopodia number (**g**) and adhesion elongation (**h**). HeLa cells transiently co-expressing RapR-Src and FRB were imaged every 2 min before and after addition of rapamycin. Membrane and adhesions were visualized as in **Figure 1**. Data are smoothed as a running average using a Gaussian filter. Unsmoothed data showing 90% confidence intervals is presented in **Supplementary Figures 10–15**. Number of cells analyzed: For RapR-Src area and rate of change, 56; protrusive activity, 31; filopodia, 23, focal adhesion analysis, 22; for G2A RapR-Src with FRB area and rate of area change, 57; protrusive activity, 42; filopodia, 25; focal adhesion, 15; for G2A RapR-Src with myristoylated FRB area and rate of area change, 39; protrusive activity, 29; filopodia, 18; focal adhesions, 21.

RapRTAP analogs of FAK and p130Cas

To examine the role of Src interactions in morphodynamics, we needed to be sure that Src interactions relevant to morphodynamics could only occur through our addition of rapamycin. We therefore examined the effects of mutations in the Src SH2 domain (R175L) and SH3 domain (W118A) to better understand downstream protein interactions and eliminate the ability of RapR Src to induce morphodynamics. Mutation of the SH2 domain alone eliminated all of the effects we had observed when simply activating Src (**Supplementary Figs. 16–21**), whereas mutation of the SH3 domain was only partially effective (**Supplementary Figs. 16–21**). Src phosphorylation of paxillin, which interacts with the Src SH3 domain, occurred at reduced levels even after the Src SH2 R175L mutation, but this was not sufficient to produce quantifiable phenotypes (**Supplementary Figs. 6** and **22**). Control studies showed that neither the SH2 nor the SH3 mutations affected catalytic activity (**Supplementary Fig. 9**).

Having learned that Src interactions mediated through its SH2 domain are critical for induction of morphological changes, we decided to focus on proteins whose interactions are mediated by this domain, specifically FAK and p130Cas. Mutation of the p130Cas sites phosphorylated by Src have clear effects on cell motility[12], and the Src–FAK interaction is known to be important for regulating cell adhesion dynamics[3,11].

To generate RapR-TAP analogs for Src–FAK and Src–p130Cas, we created chimeras of FAK and p130Cas wherein the binding site for the Src SH2 domain was replaced by the FRB domain (insertion at FAK Tyr397 (ref. 21) and p130Cas Tyr668 (ref. 22)). Addition of rapamycin would lead to activation of RapR-Src[R175L] only when it was interacting with the modified FAK or p130Cas (**Fig. 3a**). The RapR-Src R175L mutation prevented interaction with endogenous binding partners. Assays based on coexpression of RapR-Src with either FAK-FRB or p130Cas-FRB, followed by immunoprecipitation and western blotting, showed that RapR Src was activated when in complex with FAK-FRB or p130Cas-FRB; rapamycin induced a robust increase in FAK-FRB and p130Cas-FRB tyrosine phosphorylation (**Supplementary Fig. 23**). The modifications of p130Cas and FAK did not affect their subcellular localization (**Supplementary Fig. 24**).

Activation of RapR–Src[R175L] led to robust RapR–Src autophosphorylation and had no effect on the autophosphorylation of endogenous Src (**Supplementary Fig. 22**). RapR–Src[R175L] alone was unable to change the phosphorylation of endogenous FAK or p130Cas (**Supplementary Fig. 25**). Previous studies indicate that phosphorylation of p130Cas occurs downstream of Src–FAK interaction[23]. Indeed, we saw phosphorylation of endogenous p130Cas in response to activation of the Src–FAK complex, whereas formation of Src–p130Cas did not lead to phosphorylation of endogenous FAK (**Supplementary Fig. 25**).

Dissecting the roles Src–FAK and Src–p130Cas

With the RapRTAP analogs of p130Cas and FAK in hand, we could differentiate the roles of each protein in Src-induced morphodynamics. Expression of RapR-Src[R175L] with either p130Cas-FRB or FAK-FRB produced different subsets of the behaviors induced simply by Src activation: Src complexed with p130Cas, but not with FAK, generated filopodia and increased their length (**Fig. 3b,c** and **Supplementary Figs. 26** and **27**). The Src–p130Cas complex was also much more effective at increasing adhesion number than the Src–FAK complex (**Fig. 3d** and **Supplementary Fig. 28**). In contrast, Src–p130Cas had little effect on adhesion morphology, whereas Src–FAK produced an exaggerated version of the adhesion elongation that had been produced by Src alone. Adhesions became long and wispy, with less distinct borders. These adhesions were difficult to segment using automated image analysis, so naive observers were asked to score movies for adhesion morphology. (**Fig. 3e–g** and **Supplementary Video 7**). Both Src–FAK and Src–p130Cas generated cell spreading, but only p130Cas produced the limited burst of protrusion seen upon simple Src activation (**Fig. 3h–j** and **Supplementary Figs. 29–31**). FAK activation led to slower spreading and prolonged protrusive activity.

DISCUSSION

We first used RapR Src for simple activation of Src, allowing it to interact with multiple effectors. Morphological changes triggered specifically by Src are frequently studied using overexpression of constitutively active Src mutants, but this can only reveal
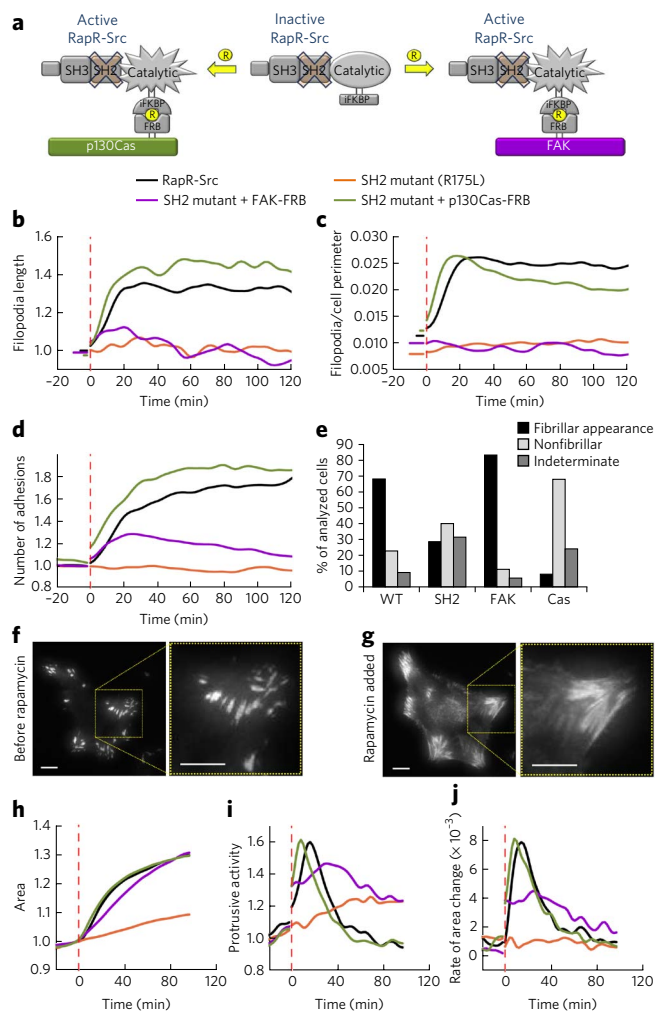
Figure 3 | Activation of specific Src-protein complexes. (**a**) The Src SH2 mutant (R175L) interacted with either p130Cas or FAK only upon rapamycin addition. Activation was restricted to the target that bore FRB. (**b–j**) Effects on filopodia length (**b**), number of filopodia (**c**), adhesion formation (**d**) and adhesion rearrangement (WT, wild type) (**e**). (**f,g**) Focal adhesions before (**f**) and after (**g**) activation of the Src–FAK complex. (**h–j**) Effects on cell area (**h**), protrusive activity (**i**) and rate of cell area change (**j**). For analysis of adhesion morphology, mCherry-tagged paxillin was used as a marker of focal adhesions. Analysis was performed as described in **Figure 2**. Unsmoothed data showing 90% confidence intervals is presented in **Supplementary Figures 26–31**. Number of cells analyzed: for RapR-Src area and rate of change, 56; protrusive activity, 31; filopodia, 23; focal adhesion analysis, 22; for SH2 mutant (R175L) area and rate of area change, 76; protrusive activity, 49; filopodia, 23; focal adhesion, 35; for SH2 mutant with FAK-FRB area and rate of area change, 73; protrusive activity, 35; filopodia analysis, 26; focal adhesions, 20; for SH2 mutant with p130Cas-FRB area and rate of area change, 73; protrusive activity, 44; filopodia, 22; focal adhesions, 25.

phenotypes that occur after prolonged exposure to elevated Src activity. RapR-Src revealed morphological changes occurring within minutes after activation, before genetic compensation could occur, and provided essentially absolute specificity, unlike drug treatments. RapR Src activation demonstrated that Src alone is sufficient to drive both lamellipodia and filopodia formation, and that it alone is capable of coordinating membrane protrusion and focal adhesions during cell spreading.

Next, RapRTAP was used to target Src activation to the cytoplasm versus the plasma membrane, suggesting a mechanism for

coordination of Src-induced protrusion and adhesion. Src could generate protrusions even without membrane anchoring, but these protrusions did not cease even after prolonged activation and did not result in stable spreading. In contrast, membrane-anchored Src did lead to spreading and was required for formation of new adhesions. This suggests that Src drives protrusion until adhesions are formed; these adhesions then inhibit further Src-induced protrusions and stabilize nascent adhesions. This mechanism is consistent with previous studies showing coordination of adhesion dynamics and protrusion at the leading edge[24].

Finally, RapRTAP clearly differentiated cell behaviors induced by Src complex formation with FAK or with p130Cas, leading to a model of the potential synergy between these two interactions (**Fig. 4**). The ability to activate a kinase while restricting activity to a specific target enables dissection of phenotypes produced by specific interactions and, as in our demonstration that the Src–FAK complex leads to phosphorylation of endogenous p130Cas, can be used to examine whether downstream events are the result of direct or indirect interactions with upstream proteins. Normal spreading was produced only through Src–p130Cas signaling. Also, only the p130Cas interaction could produce both protrusions and new adhesions to stabilize these protrusions (**Fig. 4**). When Src–FAK activation generated protrusions (with minimal adhesion formation), protrusive activity did not cease, suggesting that signals from the new adhesions might inhibit further protrusion. Once adhesions were formed, FAK but not p130Cas was shown to have a role in adhesion maturation.

Src produced filopodia via a pathway that required p130Cas but not FAK (**Fig. 4**). This is, to our knowledge, the first demonstration that Src can stimulate filopodia through p130Cas. p130Cas but not FAK has been shown to localize to the tips of filopodia[25], suggesting that p130Cas may mediate recruitment of Src for filopodia formation. Direct interaction of Src and p130Cas is most likely required for filopodia formation; we demonstrated that Src–FAK activation leads to phosphorylation of endogenous p130Cas, but this was not sufficient to produce filopodia.

In summary, we have described an approach to activate specific kinase-induced signaling pathways in living cells (RapRTAP), combining rapid and specific kinase activation with targeted protein interaction or targeted subcellular localization. It revealed different roles for Src–FAK and Src–p130Cas protein complexes in early stages of Src-induced morphodynamics. Structural studies of RapR kinases indicate that this will be a broadly applicable approach[13,26], capable of dissecting multiple kinase signaling networks *in vivo*.
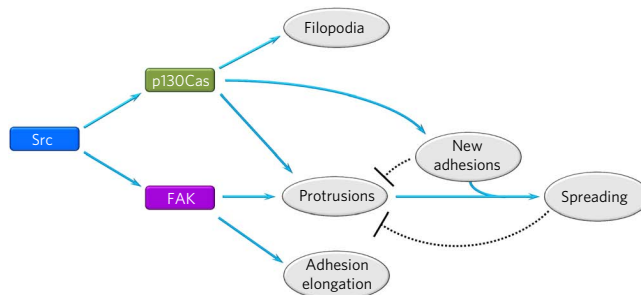

Figure 4 | Model for the role of different Src-effector interactions. Src–p130Cas generates filopodia, and Src–FAK causes adhesion elongation. Both Src–130Cas and Src–FAK produce protrusion, but Src–FAK produces unceasing protrusion-retraction cycles with no stable increase in area, whereas Src–p130Cas generates cell spreading. Src–p130Cas is more effective at producing adhesions, potentially explaining the differences between protrusions induced by Src–FAK versus Src–p130Cas. Adhesion may enable protrusion to result in cell spreading, and feedback from adhesions may halt protrusive activity.

METHODS
Methods and any associated references are available in the online version of the paper.

References

1. Thomas, S.M. & Brugge, J.S. Cellular functions regulated by Src family kinases. *Annu. Rev. Cell Dev. Biol.* **13**, 513–609 (1997).
2. Frame, M.C. Src in cancer: deregulation and consequences for cell behaviour. *Biochim. Biophys. Acta* **1602**, 114–130 (2002).
3. Playford, M.P. & Schaller, M.D. The interplay between Src and integrins in normal and tumor biology. *Oncogene* **23**, 7928–7946 (2004).
4. Cross, F.R., Garber, E.A., Pellman, D. & Hanafusa, H. A short sequence in the p60src N terminus is required for p60src myristylation and membrane association and for cell transformation. *Mol. Cell. Biol.* **4**, 1834–1842 (1984).
5. Buss, J.E., Kamps, M.P. & Sefton, B.M. Myristic acid is attached to the transforming protein of Rous sarcoma virus during or immediately after synthesis and is present in both soluble and membrane-bound forms of the protein. *Mol. Cell. Biol.* **4**, 2697–2704 (1984).
6. Dhar, A. & Shukla, S.D. Involvement of pp60c-src in platelet-activating factor-stimulated platelets. Evidence for translocation from cytosol to membrane. *J. Biol. Chem.* **266**, 18797–18801 (1991).
7. Weernink, P.A. & Rijksen, G. Activation and translocation of c-Src to the cytoskeleton by both platelet-derived growth factor and epidermal growth factor. *J. Biol. Chem.* **270**, 2264–2267 (1995).
8. Resh, M.D. & Erikson, R.L. Highly specific antibody to Rous sarcoma virus src gene product recognizes a novel population of pp60v-src and pp60c-src molecules. *J. Cell Biol.* **100**, 409–417 (1985).
9. Calothy, G. *et al.* The membrane-binding domain and myristylation of p60v-src are not essential for stimulation of cell proliferation. *J. Virol.* **61**, 1678–1681 (1987).
10. Brown, M.T. & Cooper, J.A. Regulation, substrates and functions of src. *Biochim. Biophys. Acta* **1287**, 121–149 (1996).
11. Webb, D.J. *et al.* FAK-Src signalling through paxillin, ERK and MLCK regulates adhesion disassembly. *Nat. Cell Biol.* **6**, 154–161 (2004).
12. Shin, N.Y. *et al.* Subsets of the major tyrosine phosphorylation sites in Crk-associated substrate (CAS) are sufficient to promote cell migration. *J. Biol. Chem.* **279**, 38331–38337 (2004).
13. Karginov, A.V., Ding, F., Kota, P., Dokholyan, N.V. & Hahn, K.M. Engineered allosteric activation of kinases in living cells. *Nat. Biotechnol.* **28**, 743–747 (2010).
14. Karginov, A.V. & Hahn, K.M. Allosteric activation of kinases: design and application of RapR kinases. *Curr. Prot. Cell Biol.* **53**, 14.13 (2011).
15. Kmiecik, T.E. & Shalloway, D. Activation and suppression of pp60c-src transforming ability by mutation of its primary sites of tyrosine phosphorylation. *Cell* **49**, 65–73 (1987).
16. Berginski, M.E., Vitriol, E.A., Hahn, K.M. & Gomez, S.M. High-resolution quantification of focal adhesion spatiotemporal dynamics in living cells. *PLoS ONE* **6**, e22025 (2011).
17. Bjorge, J.D., Jakymiw, A. & Fujita, D.J. Selected glimpses into the activation and function of Src kinase. *Oncogene* **19**, 5620–5635 (2000).
18. Sandilands, E., Brunton, V.G. & Frame, M.C. The membrane targeting and spatial activation of Src, Yes and Fyn is influenced by palmitoylation and distinct RhoB/RhoD endosome requirements. *J. Cell Sci.* **120**, 2555–2564 (2007).
19. Kamps, M.P., Buss, J.E. & Sefton, B.M. Mutation of NH2-terminal glycine of p60src prevents both myristoylation and morphological transformation. *Proc. Natl. Acad. Sci. USA* **82**, 4625–4628 (1985).
20. Pellman, D., Garber, E.A., Cross, F.R. & Hanafusa, H. Fine structural mapping of a critical NH2-terminal region of p60src. *Proc. Natl. Acad. Sci. USA* **82**, 1623–1627 (1985).
21. Schaller, M.D. *et al.* Autophosphorylation of the focal adhesion kinase, pp125FAK, directs SH2-dependent binding of pp60src. *Mol. Cell. Biol.* **14**, 1680–1688 (1994).
22. Nakamoto, T., Sakai, R., Ozawa, K., Yazaki, Y. & Hirai, H. Direct binding of C-terminal region of p130Cas to SH2 and SH3 domains of Src kinase. *J. Biol. Chem.* **271**, 8959–8965 (1996).
23. Cary, L.A., Han, D.C., Polte, T.R., Hanks, S.K. & Guan, J.L. Identification of p130Cas as a mediator of focal adhesion kinase–promoted cell migration. *J. Cell Biol.* **140**, 211–221 (1998).
24. Parsons, J.T., Horwitz, A.R. & Schwartz, M.A. Cell adhesion: integrating cytoskeletal dynamics and cellular tension. *Nat. Rev. Mol. Cell Biol.* **11**, 633–643 (2010).
25. Gustavsson, A., Yuan, M. & Fallman, M. Temporal dissection of β1-integrin signaling indicates a role for p130Cas-Crk in filopodia formation. *J. Biol. Chem.* **279**, 22893–22901 (2004).
26. Dagliyan, O. *et al.* Rational design of a ligand-controlled protein conformational switch. *Proc. Natl. Acad. Sci. USA* **110**, 6800–6804 (2013).

Author contributions
A.V.K. and K.M.H. initiated the project, and A.V.K. carried out the bulk of the experimental studies. D.T. and T.C.E. developed and applied the new method used to analyze filopodia dynamics. M.B. and S.G. quantified cell adhesion dynamics. All of the other morphodynamic quantifications were by D.T. and A.V.K. E.D.T. and P.-H.C. assisted with kinase assays and cloning. J.J.Y. provided mCherry-stargazin. All of the authors contributed to the writing of the manuscript.

Competing financial interests
The authors declare no competing financial interests.

Additional information
Supplementary information is available in the online version of the paper. Reprints and permissions information is available online at http://www.nature.com/reprints/index.html. Correspondence and requests for materials should be addressed to K.M.H.

ONLINE METHODS

Data analysis. Data in **Figures 1–3** are smoothed by running average using a Gaussian filter. The unsmoothed data, with error bars, and statistical analysis of the data are provided in **Supplementary Figures 4**, **5**, **11–13**, **15**, **17**, **18**, **21**, **26** and **28–31**.

Antibodies and reagents. Anti-phospho-paxillin (Tyr31) (cat. no. 44-720G), anti-phospho-Src (Tyr418) (cat. no. 44660G) and anti-phospho-FAK (Tyr397) (cat. no. 44624G) antibodies were purchased from Invitrogen. Anti-GFP antibodies were purchased from Clontech (cat. no. 632380). Anti-phosphotyrosine (4G10) (cat. no. 05-321), anti-myc antibodies (cat. no. 05-724) and IgG-coupled agarose beads (cat. no. IP04-1.5ML) were purchased from Millipore. Anti-p130Cas (cat. no. 12015), anti-phospho-p130Cas (Tyr410) (cat. no. 4011), anti-FAK (cat. no. 3285) and anti-Src (cat. no. 2108) antibodies were purchased from Cell Signaling Technology. Anti-paxillin antibodies were a gift from M. Schaller (West Virginia University). All of the antibodies were used at a 1:1,000 dilution. Rapamycin was purchased from LC Laboratories. All of the restriction enzymes were purchased from New England BioLabs.

Molecular biology. GFP-paxillin, mCherry-paxillin, GFP-FAK, mCherry-FAK, RapR-Src-myc, mCherry-FRB and GFP-FRB constructs were previously described[13]. To generate pmVenus-p130Cas, the p130Cas gene was cut out of a pEBG-p130Cas plasmid (purchased from AddGene, provided by R. Birge (Rutgers University)) using BamHI and NotI and then was ligated with pmVenus-CI vectors predigested with BglII and PspOMI. RapR-Src-Cerulean-myc and RapR-Src-GFP-myc constructs were generated by insertion of GFP and Cerulean genes into the RapR-Src-myc construct using a modification of site-directed mutagenesis, as previously described[14]. The mVenus-FAK construct was generated by replacing the GFP in the GFP-FAK construct with mVenus using a modification of site-directed mutagenesis, as previously described[13,14]. mVenus-FAK-FRB and mVenus-p130Cas-FRB constructs were generated by insertion of FRB into mVenus-FAK (replacing Tyr397 codon) and mVenus-p130Cas (replacing Tyr668 codon) using a modification of site-directed mutagenesis as previously described[13,14]. Myristoylated mCherry-FRB and GFP-FRB constructs were generated by insertion of the N-terminal myristoylation fragment of Src (encoding first 11 amino acids) at the N terminus of mCherry and GFP in mCherry-FRB and GFP-FRB, using a modification of site-directed mutagenesis, as previously described[13,14]. G2A, W118A, R175L and Y529F mutations of RapR-Src were performed using a site-directed mutagenesis method (QuikChange site-directed mutagenesis protocol, Agilent Technologies). To generate the stargazin-mCherry construct, the stargazin gene was PCR amplified from mouse stargazin cDNA and ligated into pmCherry-N1 using XhoI and BamHI sites. A multiple cloning site was also introduced into the intracellular loop of stargazin through PCR.

Cell imaging. Cells were plated on fibronectin-coated coverslips (5 mg/L fibronectin) 2–4 h before imaging, then transferred into L-15 imaging medium (Invitrogen) supplemented with 5% FBS. Live cell imaging was performed in an open heated chamber (Warner Instruments) using an Olympus IX-81 microscope equipped with an objective-based total internal reflection fluorescence (TIRF) system and a PlanApo N 60× TIRFM objective (NA 1.45) or a UPlanFLN 40× (Oil, NA 1.30) objective. All of the images were collected using a Photometrix CoolSnap ES2 CCD camera controlled by Metamorph software. A 440-nm laser from Kimmon Koha (Ik Series He-Cd, model IK4171I-G), a 491-nm laser from Olympus (Cell TIRF 491 laser, model LAS/491/50) and a 594-nm laser from Cobolt (model Mambo) were used for TIRF imaging. Epifluorescence images were taken using a high-pressure mercury arc light source.

Cell spreading and protrusive activity analysis. We used the neuronal tetraspanin molecule stargazin to label the plasma membrane in our studies. Endogenous stargazin expression in heterologous cells is very low[27], and previous studies have shown that expression of fluorescent protein–tagged stargazin results in uniform labeling of the plasma membrane[28]. The RapR-Src construct had a Y529F mutation in the C terminus of Src that prevented regulation of RapR-Src by upstream signaling pathways. Cells expressing RapR-Src-Cerulean constructs, stargazin-mCherry and GFP-FRB were selected using epifluorescence imaging. Time-lapse movies were taken at 2-min time intervals. Image analysis was performed using Metamorph software. A binary mask of a cell was created on the basis of Stargazin-mCherry images and used to assess cell area. To calculate the cell area change, we divided the cell area at the given time

point by the area of the same cell at the time point immediately before addition of rapamycin. The following number of cells were analyzed: 56 cells for RapR-Src, 47 cells for the kinase-dead mutant (D388R) of RapR-Src, 36 cells for the control without RapR-Src, 49 cells for the SH3 domain mutant (W118A) of RapR-Src, 57 cells for the myristoylation mutant (G2A) of RapR-Src, 39 cells for activation of the G2A mutant of RapR-Src at the plasma membrane with myristoylated FRB, 76 cells for the SH2 domain mutant (R175L) of RapR-Src, 73 cells for activation of the R175L mutant of Src in complex with FAK-FRB and 73 cells for activation of the R175L mutant of RapR-Src in complex with p130Cas. To calculate the protrusive activity of the cell, we first calculated the sum of the areas associated with regions of the cell that undergo local extensions between subsequent movie frames. We refer to this area as the protrusive area. Then, to determine fold change in protrusive activity, we divided the protrusive area during each time interval by the time-averaged protrusive area before the addition of rapamycin. The following numbers of cells were analyzed: 31 cells for RapR-Src, 21 cells for the kinase-dead mutant (D388R) of RapR-Src, 36 cells for the control without RapR-Src, 49 cells for the SH3 domain mutant (W118A) of RapR-Src, 42 cells for the myristoylation mutant (G2A) of RapR-Src, 29 cells for activation of the G2A mutant of RapR-Src at the plasma membrane with myristoylated FRB, 49 cells for the SH2 domain mutant (R175L) of RapR-Src, 35 cells for activation of the R175L mutant of Src in complex with FAK-FRB and 44 cells for activation of the R175L mutant of RapR-Src in complex with p130Cas.

Filopodia analysis. To quantify filopodia dynamics from time-lapse movies, we used a computational method that allows accurate identification and tracking of all cellular protrusions for cells and protrusions of arbitrarily complex shape[29] (**Supplementary Fig. 2**). Briefly, the steps involved in the process include:

(i) Mapping the cell outline onto a tree graph. In general, an arbitrary closed (non-self-intersecting) polygonal chain can be mapped to a tree graph using a medial axis transform (MAT)[30–33]. The branches of the tree emanate from a single point inside the cell (the root of the tree) and eventually reach each point of the cell boundary. Thus, every boundary point is connected to a common origin through a unique path on the graph that always remains inside the cell, regardless of the complexity of the cell shape (**Supplementary Fig. 2a**). The root can be defined as the cell center, but it does not coincide with the centroid. It coincides with the center of the largest possible circle that can be inscribed within the cell boundary.

(ii) Boundary profiling. Plotting the distance along each graph path from the root to the boundary as a function of the boundary points provides a mechanism for identifying protrusions. In the graph in **Supplementary Figure 2c**, the protrusion tips appear as local maxima.

(iii) Filopodia detection. The path that starts at the protrusion tip and runs through the center of the protrusion can be used to calculate protrusion length, whereas the short branches from these central lines to the boundary provide a measure of the protrusion width. Filopodia are defined by specifying cut-off values for the width and length of the protrusions (**Supplementary Fig. 2b**). In this way, we make sure that the algorithm selects only thin filopodia-like protrusions.

(iv) Filopodia tracking. The skeleton segments from the previous step not only allow us to define filopodia but also provide a reliable method for tracking these protrusions over time and quantify their dynamic behavior. One important improvement of the algorithm, made specifically for the presented here analysis, was to include automated differentiation of active (dynamic) filopodia from passive structures resulting from cell retraction. This modification allowed us to increase the accuracy of filopodia quantification by avoiding overestimation due to retraction fibers at the cell edge.

The following number of cells were analyzed: 23 cells for RapR-Src, 23 cells for the kinase-dead mutant (D388R) of RapR-Src, 33 cells for the control without RapR-Src, 22 cells for SH3 domain mutant (W118A) of RapR-Src, 25 cells for myristoylation mutant (G2A) of RapR-Src, 18 cells for activation of G2A mutant of RapR-Src at the plasma membrane with myristoylated FRB, 23 cells for SH2 domain mutant (R175L) of RapR-Src, 26 cells for activation of R175L mutant of Src in complex with FAK-FRB and 22 cells for activation of R175L mutant of RapR-Src in complex with p130Cas.

Focal adhesion analysis. Analysis of focal adhesions was performed as previously described[16,34]. To determine focal adhesion number and elongation after rapamycin addition, we first calculated the average value of the property across all of the identified adhesions in each image, producing a time series for each time-lapse image set. Each time series was normalized so that the value immediately before rapamycin addition was equal to one. The following number of cells were analyzed: 22 cells for RapR-Src, 18 cells for the kinase-dead mutant (D388R) of RapR-Src, 27 cells for the SH3 domain mutant (W118A) of RapR-Src, 15 cells for the myristoylation mutant (G2A) of RapR-Src, 21 cells for activation of the G2A mutant of RapR-Src at the plasma membrane with myristoylated FRB, 35 cells for the SH2 domain mutant (R175L) of RapR-Src, 20 cells for activation of the R175L mutant of Src in complex with FAK-FRB and 25 cells for activation of the R175L mutant of RapR-Src in complex with p130Cas.

27. Choi, J. *et al.* Phosphorylation of stargazin by protein kinase A regulates its interaction with PSD-95. *J. Biol. Chem.* **277**, 12359–12363 (2002).
28. Chen, L. *et al.* Stargazin regulates synaptic targeting of AMPA receptors by two distinct mechanisms. *Nature* **408**, 936–943 (2000).
29. Tsygankov, D. *et al.* CellGeo: a computational platform for the analysis of shape changes in cells with complex geometries. *J. Cell Biol.* **204**, 443–460 (2014).
30. Lee, D.T. Medial axis transformation of a planar shape. *IEEE Trans. Pattern Anal. Mach. Intell.* **4**, 363–369 (1982).
31. Blum, H. in *Models for the Perception of Speech and Visual Form* (ed. Dunn, W.W.) 362–380 (MIT Press, 1967).
32. Chin, F., Snoeyink, J. & Wang, C.A. Finding the medial axis of a simple polygon in linear time. *Discrete Comput. Geom.* **21**, 405–420 (1999).
33. Aichholzer, O. *et al.* Medial axis computation for planar free-form shapes. *Comput. Aided Des.* **41**, 339–349 (2009).
34. Wu, C. *et al.* Arp2/3 is critical for lamellipodia and response to extracellular matrix cues but is dispensable for chemotaxis. *Cell* **148**, 973–987 (2012).

Dissecting motility signaling through activation of specific Src-effector complexes

Andrei V Karginov, Denis Tsygankov, Matthew Berginski, Pei-Hsuan Chu, Evan D Trudeau, Jason J Yi, Shawn Gomez, Timothy C Elston & Klaus M Hahn

Nat. Chem. Biol. **10**, 286–290 (2014); published online 9 March 2014; corrected after print 7 April 2014

In the version of this article initially published online, the colors of the purple (SH2 mutant + FAK-FRB) and green (SH2 mutant + p130Cas-FRB) curves in Figure 3d were swapped, leading to a mislabeling of the two experimental results. The error has been corrected for the PDF and HTML versions of this article.